Title
Quantitative Evaluation of the In Vivo Vocal Fold Medial Surface Shape

Journal
Journal of Voice, 31(4)

ISSN
0892-1997

Authors
Vahabzadeh-Hagh, Andrew M
Zhang, Zhaoyan
Chhetri, Dinesh K

Publication Date
2017-07-01

DOI
10.1016/j.jvoice.2016.12.004

Peer reviewed

HHS Public Access

Author manuscript

J Voice. Author manuscript; available in PMC 2018 July 01.

Published in final edited form as:

J Voice. 2017 July ; 31(4): 513.e15–513.e23. doi:10.1016/j.jvoice.2016.12.004.

Quantitative Evaluation of the *In Vivo* Vocal Fold Medial Surface Shape

Andrew M. Vahabzadeh-Hagh, **Zhaoyan Zhang**, and **Dinesh K. Chhetri**

Department of Head and Neck Surgery, David Geffen School of Medicine at UCLA, Los Angeles, California

Summary

Objectives/Hypothesis—Glottal insufficiency is a common clinical problem in otolaryngology and medialization laryngoplasty (ML) procedures remain the primary treatment modality. Although the goal of ML is to restore physiologic glottal posture and achieve optimal phonation, this posture has not been directly measured. In this study, we assessed glottal medial surface contour changes with selective activation of the intrinsic laryngeal muscles (ILMs).

Study Design—Basic science study using an *in vivo* canine hemilarynx model.

Methods—In an *in vivo* canine hemilarynx, India ink was used to mark fleshpoints in a grid-like fashion along the medial surface of the vocal fold and ILMs were activated in a graded manner. A right-angled prism provided two views of the medial surface, which were recorded using a high-speed camera and used to reconstruct the 3D posture deformations of the medial surface.

Results—Thyroarytenoid (TA) muscle activation results in initial inferomedial bulging and increased glottal channel thickness and then glottal adduction with a final rectangular glottal channel shape. Lateral cricoarytenoid (LCA) activation closes the posterior glottis but final posture remains slightly convergent. Together, TA + LCA forms a rectangular glottis with an increased glottal vertical thickness. Posterior cricoarytenoid activation results in abduction and a slightly divergent glottis, whereas cricothyroid activation elongates the glottis and reduces the glottal channel vertical thickness.

Conclusions—A quantitative analysis of *in vivo* canine vocal fold medial surface upon activation of selective ILMs is provided. This may guide our therapeutic efforts during medialization laryngoplasty, as well as computational modeling of laryngeal physiology.

Keywords

Larynx; Canine; Vocal fold; Prephonatory posture; Vocal fold medial surface shape

Address correspondence and reprint requests to Andrew M. Vahabzadeh-Hagh, Department of Head and Neck Surgery, David Geffen School of Medicine at UCLA, 10833 Le Conte Ave, 62-132 CHS, Los Angeles, CA 90095. AVahabzadehHagh@mednet.ucla.edu.

Presented as an oral presentation at the Triological Society Combined Sections Meeting, Miami Beach, Florida, USA, January 22–24, 2016.

Conflict of interest: None.

INTRODUCTION

During phonation, the glottal vibratory mode and phonation type depends upon the magnitude of subglottal pressure and vocal fold properties such as stiffness, longitudinal tension, and prephonatory geometry. The prephonatory geometry, specifically the geometry of the medial surface of the vocal fold, directly affects glottal fluid-structure interaction and is a critical parameter controlling the phonatory types and effort. Previous studies showed that an optimal medial surface geometry may exist, achieving the lowest phonation threshold pressure.[1–3]

The prephonatory glottal geometry is shaped by actions of three pairs of intrinsic laryngeal muscles (ILMs).[4,5] The thyroarytenoid (TA) forms the physical bulk of the glottis and upon contraction causes shortening, medial bulging, and adduction of the membranous vocal folds and imparts stiffness to the body layer. The lateral cricoarytenoid (LCA) muscle adducts the vocal fold at its attachment to the vocal process, achieving posterior glottal closure. The cricothyroid (CT) muscle elongates the vocal fold. The effects of ILMs on glottal channel shape have been primarily investigated from the superior endoscopic view of the larynx. However, glottal shape changes are three-dimensional with the medial surface critical to voice production but hidden from a superior view. A gap in knowledge of how the glottal medial surface varies during phonation exists, largely resulting from our inability to directly visualize the medial surface of the vocal folds *in vivo*. A precise knowledge of the medial surface contour under conditions of individual ILM activation would allow improved modeling of voice production and implant design in vocal fold medialization. A systematic investigation of vocal fold medial surface geometry under different laryngeal muscle activation conditions is warranted.

In this investigation, we systematically quantified the 3D glottal channel geometry upon activation of ILMs in a neuromuscularly intact *in vivo* canine larynx model. We evaluated the effects on the medial surface shape induced by each ILM from baseline to full activation, as well as the interactions between the TA and LCA muscles in shaping glottal channel prephonatory posture.

METHODS

This study was approved by the Institutional Animal Care and Use Committee. One mongrel canine was used. The larynx was exposed and exteriorized in the neck as previously described.[4,5] Briefly, a vertical midline skin incision was made to provide wide exposure of the laryngotracheal framework. Tracheostomy tube was placed and the oral endotracheal tube was removed. Infrahyoid pharyngotomy and circumferential division of the pharynx allowed for mobilization and exteriorization of the larynx into the neck. We then removed the bilateral false vocal folds and epiglottis. Subsequently, a right hemilaryngectomy was performed to expose the left vocal fold and India ink was used to mark fleshpoints spaced approximately 1.3 mm apart (each fleshpoint was 130 to 220 microns in diameter) in a grid-like fashion along the medial surface of the left vocal fold. The hypotenuse of a right-angle glass prism was placed along the anatomic midline of the glottis from the anterior to the posterior commissure. The prism provided two distinct medial vocal fold views for a high-

speed digital camera placed perpendicular to the glottal midline. This hemilaryngeal setup is shown in Figure 1.

Mapping functions for 3D analysis were calculated by calibrating the camera (384 × 672 pixel resolution; 0.04 mm/pixel) to a standardized calibration plate with known 3D coordinates as previously described (25 × 25 mm calibration target, LaVision Inc., Type no. 2.5, Version 7.2, Goettingen, Germany).[6] These mapping functions are used to calculate the surface height along the medial surface of the vocal fold allowing 3D reconstruction of the medial surface contour (Figure 2). The software uses both the fleshpoints and finer random surface pixel variation, as long as they are of adequate high-pattern contrast, for image correlation and surface adaptation. Here, more high-contrast points per correlation window provide better surface approximation. Because the fleshpoints were spaced 30 pixels apart and the correlation window was 64 × 64 pixels, one window always included six to nine fleshpoints at any given time. We also generated correlation maps to determine the accuracy of the correlation between interrogation windows among the camera views. The correlation maps for the anterior, mid, and posterior sections of the vocal fold medial surface showed sharp peaks amid a flat background, supporting successful implementation of this correlative surface approximation method.

We used one high-speed camera to obtain stereo or 3D images of the vocal fold medial surface. Thus, the stereo angle, or separation angle between camera views, was limited by our prism selection. Although a 60-degree prism may have provided a more optimal distribution of multidimensional error in our measurements, we elected to use a right-angle prism given prior successes in capturing the full range of medial-lateral motion of the vocal fold and that use of a more acute-angle prism could result in larger error in measurements of glottal width.[7–11]

Each ILM was activated via neuromuscular stimulation of respective nerve branches. The recurrent laryngeal nerve was identified, and branches to the posterior cricoarytenoid (PCA) and TA were ligated and each distal end attached to a cuff electrode for stimulation. After the TA branch was divided, a cuff electrode was placed around the recurrent laryngeal nerve trunk for LCA/Interarytenoid (IA) muscle complex stimulation. The branches of the superior laryngeal nerve were identified, the internal (sensory) branch was ligated, and a cuff electrode was applied to the external (motor) branch for CT muscle stimulation. Neuromuscular stimulation was performed at 100 Hz for 1500 ms with uniform 0.1 ms cathodic pulses. Graded activation of the ILMs was performed over 12 levels, from zero, no activation, to 11, maximally activating stimulus current. Vocal fold motion and deformation was captured at 3000 frames per second using a high-speed digital camera (Phantom v210, Vision Research Inc., Wayne, NJ). The distance from the camera to the prism and larynx was kept constant throughout. Each stimulation was followed by a 3.5-second pause to allow time for muscle recovery and data transfer.

The image-processing program DaVis (LaVision Inc.) was used for time series cross-correlation analysis for 3D deformation calculations of the medial surface during activation of individual ILMs. The surface “height” along the medial surface of the vocal fold (ie, the distance from the vocal fold surface to the prism in the midline, defined as position “0”) as

well as the “displacement” (ie, the change in surface height between consecutive frames) was exported into MATLAB (MATLAB release 2015a, The Mathworks, Inc., Natick, MA). 3D contour plots of the medial surface were used to assess location and extent of motion along the medial surface with ILM activations.

RESULTS

Glottal configuration with individual ILM full activation

The change in glottal width (medial surface distance from the glottal midline) was first assessed with 12 grades of stimulation of individual ILMs. The stimulation grade beyond which no further change in glottal width occurred was considered maximum muscle activation, and the temporal and spatial changes of the medial surface under this maximum stimulation was analyzed. Figure 3 shows glottal width changes in a color-coded format detailing the 3D deformation for each ILM under maximum activation. For each stimulation condition, we selected five frames that captured the full range of motion of the vocal fold medial surface with a reasonable interframe interval, from resting position to complete activation. With activation of the TA, inferomedial bulging of the vocal fold begins rapidly and is appreciable by 14 ms. The mid-membranous region is near fully adducted by 22 ms, whereas the entire membranous fold adducts by 47 ms. TA activation also results in anteroposterior (AP) shortening and increased vertical thickness (height) of the vocal fold medial surface. LCA activation results in adduction of the posterosuperior fold, first appreciable between 16 and 22 ms, and complete with a mid-membranous gap by 47 ms. The PCA and CT exhibit a slower time course of activation, with changes first appreciable between 16 and 33 ms, and completion around 100 ms. PCA abducts the posterosuperior edge of the vocal fold, and results in AP lengthening, vertical shortening, and height elevation. CT activation yields minor abduction, AP lengthening, vertical shortening, and lowering of the vocal fold.

Coronal sections of the vocal fold medial surfaces shown in Figure 3 at the mid-membranous fold (“Mid”) position and a position halfway between mid-fold and vocal process (“Post”) are shown in Figure 4 for the same ILMs, activation levels, and temporal sequence. The coronal view highlights the glottal channel geometry (divergent, convergent, or rectangular). Within each plot, each line represents a coronal section corresponding to the same time points for each ILM shown in Figure 3. The resting midfold coronal sections (“t0”, blue) for each muscle demonstrates a slightly convergent glottis (note that the figure axes are not in equal scale). The posterior section is more rectangular. TA activation yields rapid inferomedial bulging followed by complete adduction of the midfold, whereas the posterior segment adducts more slowly, but both end in a rectangular midline configuration. LCA leads to slower and incomplete adduction of the midfold, while full posterior closure with a slightly convergent configuration is achieved. PCA abducts the mid and posterior coronal sections while transitioning to a slightly divergent posture. CT yields minimal abduction of the mid and posterior coronal sections. The expected errors in linear measurements using our methods ranged from 12 to 20 microns, translating to an error of one degree in the angle of convergence or divergence of the coronal section.

Glottal channel configuration achieved via the interaction of the laryngeal adductors

The TA and LCA are the main vocal fold adductors and their actions are the targets for medialization procedures such as injection augmentation and type 1 thyroplasty. Figure 5 presents the medial surface displacement (eg, changes in glottal width relative to the resting glottal width) for maximal TA, LCA, and combined TA + LCA activations. These displacement plots highlight the focal point of deformation on the medial surface with ILM activation. The TA again shows fast inferomedial bulging while the LCA adducts posteriorly. The combined activation of TA + LCA shows early effects dominated by the TA with inferomedial bulging at 14 ms, followed by combined inferomedial and posterosuperior adduction at 16 ms. Enhanced adduction is appreciated throughout the remaining posture changes.

To illustrate the individual and combined effects of TA and LCA on medial surface geometry, Figure 6 shows coronal sections for submaximal activation of the TA (“TA 2”) and LCA (“LCA 3”), and maximal activation of the TA-LCA combination (“TA-LCA”). TA causes mid to inferomedial bulging (black arrow denotes point of maximal adduction), whereas the LCA provides more superior medialization of the vocal fold (gray arrow denotes point of maximal adduction). With combined maximal TA and LCA activation (“TA-LCA”), we observe a combined superior and inferomedial adduction, the combination of which achieves a more rectangular glottal configuration.

Temporal patterns of vocal fold medial surface change with graded stimulation

Figure 7 demonstrates the percent of maximal adduction achieved for each grade of stimulation for each ILM. The TA was most responsive to graded stimulation, achieving maximum percent displacement at stimulus levels 4–5, and leveling off at level 7. The LCA and PCA exhibited more gradual and linear responses to increased stimulus grade. The percent displacement was minimal for CT. The lower panel shows posterior fold displacement mirroring that of the midfold, except for a slower TA rise time and more responsive LCA.

Figure 8 shows the changes in glottal width (displacement) for each ILM for each grade of stimulation as a function of time. This illustrates vocal fold speed at the mid and posterior vocal fold as a function of grade of stimulation. The TA demonstrates the fastest response of the midfold achieving maximal adduction within 20 ms for the highest stimulus level. These speeds are reduced for the posterior fold but still the fastest among other ILMs. The LCA also demonstrates faster adduction without saturating for increasing stimulus level, with the greatest effect on the posterior fold. Similarly, the PCA shows faster abduction with increasing stimulus over a longer time course. The CT again exhibits minimal effect of stimulus on changes in glottal width. Overall, these curves demonstrate that a given glottal width at the mid or posterior vocal fold can be achieved more rapidly with a higher stimulus level.

DISCUSSION

Various 2D visualization techniques such as high-speed cinematography, plain-film tomography, x-ray stroboscopy, and strobophotoglottography dating back as early as the 1940s have provided 2D views of glottal channel during vocal fold vibration.[8,12–15] They led to the development of our current understanding of the vertical phase difference and convergent to divergent cycling of the vocal folds during phonation. In 1959, Fink and Kirschner visualized the phonating human vocal folds using x-ray tomography and recorded a convex infraglottic shape, that of an exponential curve. They stated that the exponential curve-shaped glottal wall would produce the lowest coefficient of flow resistance maximizing phonatory efficiency.[13] In the 1970s and 1980s, Hirano studied the geometric influence of each ILM in excised canine larynges. While providing electrical stimulation to the TA muscle, he quickly froze the entire larynx in alcohol at −30 degrees, then fixed and sectioned it in the coronal plane. He observed adduction, bulging, and rounding of the medial surface of the vocal fold but the temporal sequence of posture changes could not be investigated with his technique.[16] In our study, we use high-speed video capture and a 3D deformation algorithm at high neuromuscular and spatial resolution to directly measure vocal fold medial surface shape changes during individual and combined ILM activation in a temporal sequence from baseline to full activation (Figures 3–6). We show that TA activation leads to inferomedial bulging and convexity of the midmembranous vocal fold, whereas the LCA provides a more superior medialization in the midfold and more complete posterior adduction.

In cases of laryngeal denervation, we aim to therapeutically recreate the ideal prephonatory posture of the glottis through injection, type I laryngoplasty, or arytenoid adduction, but what glottal geometry is ideal? This is a question that many have tried to answer, and, as a result, the way in which we do injection laryngoplasty and the shape of our thyroplasty implants have evolved.[1,17,18] Titze found that a divergent prephonatory glottal configuration achieved lower oscillation threshold pressures correlating with greater ease of phonation.[3] However, other studies using physical models and numerical studies showed that the lowest phonation threshold pressure occurs for a rectangular or slightly convergent glottis.[19–21] Orestes et al investigated acoustic and aerodynamic effects of thyroplasty implant depth and shape. They found that medial implant shape became more important with increasing depth of insertion, and favored a divergent shape.[18] Mau et al predicted that increasing vertical thickness (ie, glottal channel height) of the vocal folds and a more rectangular glottal geometry would lower phonation threshold pressure and flow.[1] Further, Courey tested injection material into different locations within the glottis and found that placement of graft in the medial aspect of the TA muscle reduced the forces necessary to bring the vocal folds into position for vibration.[17] The histology from that report also appeared to approximate a rectangular glottis. In the present study, we demonstrate the coronal configurations of the medial surface of the vocal fold through direct observation (Figure 4). We observe a rectangular or near-rectangular glottis with activation of the TA, LCA, and CT muscles, which appears to be consistent with previous studies.

In this study we also directly observe that the prephonatory posture with full combined activation of the TA and LCA yields both the inferomedial bulge (due to TA) and

posterosuperior adduction (due to LCA), resulting in a larger adducted surface area (Figure 5) and a more rectangular and thicker glottis (Figure 6). Further, we see that this rectangular and thickened glottal configuration can be approximated with submaximal stimulation of the TA and LCA. Variation of vertical thickness has important effects on the closure pattern of vocal fold vibration and the produced acoustics.[22] The vertical thickness has also been reported to affect onset threshold pressure. Chan et al reported optimal phonation threshold pressures with a thicker glottal configuration.[19] However, an opposite relationship between phonation threshold pressure and vocal fold thickness was observed by Zhang and Mendelsohn in their experiments and numerical simulations.[23–25]

TA activation is known to exhibit a sigmoidal response function over a narrow band of stimulation current.[10,26] Here, using our paradigm of graded stimulation, we, too, observed a sigmoidal activation curve for the TA, with more linear responses for LCA and PCA (Figure 7). Lastly, we observed that with increasing stimulation grade, the glottis progresses through the same schema of glottal configuration changes but does so at increasing speeds (Figure 8). This direct proportion holds true for each ILM tested, although the TA muscle has the fastest response. Thus, the TA muscle appears well suited for rapid control of glottal configuration, which may result in rapid modification of acoustic parameters such as fundamental frequency, intensity, open quotient, and phonation types.[27–29]

One limitation of this study is that we do not yet have information on the differential stiffness in the vertical dimension of the vocal fold with ILM activation, which will be pursued in our future research.

CONCLUSIONS

Direct assessment of *in vivo* vocal fold medial surface geometry with ILM activation reveals inferomedial bulging with TA activation and a rectangular, thickened glottis with combined TA and LCA activation. This information can be combined with future studies on the role of implant stiffness to improve treatment of glottic insufficiency. Detailed investigations of the interactions of ILMs on glottal prephonatory shape are also necessary to determine the ideal shape for various phonation types.

Acknowledgments

This study was supported by grants R01DC011299 and R01DC011300 from the National Institutes of Health.

The authors would like to thank Dr. Juergen Neubauer for his assistance with the experiment.

References

1. Mau T, Muhlestein J, Callahan S, et al. Modulating phonation through alteration of vocal fold medial surface contour. Laryngoscope. 2012; 122:2005–2014. [PubMed: 22865592]
2. Scherer RC, Shinwari D, De Witt KJ, et al. Intraglottal pressure distributions for a symmetric and oblique glottis with a uniform duct. J Acoust Soc Am. 2002; 112:1253–1256. [PubMed: 12398430]
3. Titze IR. The physics of small-amplitude oscillation of the vocal folds. J Acoust Soc Am. 1988; 83:1536–1552. [PubMed: 3372869]

4. Chhetri DK, Neubauer J, Bergeron JL, et al. Effects of asymmetric superior laryngeal nerve stimulation on glottic posture, acoustics, vibration. Laryngoscope. 2013; 123:3110–3116. [PubMed: 23712542]
5. Chhetri DK, Neubauer J, Berry DA. Graded activation of the intrinsic laryngeal muscles for vocal fold posturing. J Acoust Soc Am. 2010; 127:El127–El133. [PubMed: 20369979]
6. Zhang Z, Neubauer J, Berry DA. Aerodynamically and acoustically driven modes of vibration in a physical model of the vocal folds. J Acoust Soc Am. 2006; 120(5 pt 1):2841–2849. [PubMed: 17139742]
7. Abdel-Aziz, Y., Karara, H. Direct linear transformation from comparator coordinates into object space coordinates in close-range photogrammetry. ASP Symposium on Close Range Photogrammetry; 1971;
8. Berry DA, Montequin DW, Tayama N. High-speed digital imaging of the medial surface of the vocal folds. J Acoust Soc Am. 2001; 110(5 pt 1):2539–2547. [PubMed: 11757943]
9. Doellinger M, Berry DA, Berke GS. A quantitative study of the medial surface dynamics of an in vivo canine vocal fold during phonation. Laryngoscope. 2005; 115:1646–1654. [PubMed: 16148711]
10. Dollinger M, Berry DA, Berke GS. Medial surface dynamics of an in vivo canine vocal fold during phonation. J Acoust Soc Am. 2005; 117:3174–3183. [PubMed: 15957785]
11. Chen L, Armstrong CW, Raftopoulos DD. An investigation on the accuracy of three-dimensional space reconstruction using the direct linear transformation technique. J Biomech. 1994; 27:493–500. [PubMed: 8188729]
12. Farnsworth D. High-speed motion pictures of the human vocal cords. Bell Lab Rec. 1940; 18:203–208.
13. Fink BR, Kirschner F. Observations on the acoustical and mechanical properties of the vocal folds. Folia Phoniatr (Basel). 1959; 11:167–172. [PubMed: 13822887]
14. Hess MM, Ludwigs M. Strobophotoglottographic transillumination as a method for the analysis of vocal fold vibration patterns. J Voice. 2000; 14:255–271. [PubMed: 10875578]
15. Saito, S., Fukuda, H., Isohai, Y., et al. X-ray stroboscopy. In: Stevens, K., editor. Vocal Fold Physiology. Tokyo: University of Tokyo; 1981. p. 95-106.
16. Hirano M. Vocal mechanisms in singing: laryngological and phoniatric aspects. J Voice. 1988; 2:51–69.
17. Courey MS. Homologous collagen substances for vocal fold augmentation. Laryngoscope. 2001; 111:747–758. [PubMed: 11359151]
18. Orestes MI, Neubauer J, Sofer E, et al. Phonatory effects of type I thyroplasty implant shape and depth of medialization in unilateral vocal fold paralysis. Laryngoscope. 2014; 124:2791–2796. [PubMed: 25046146]
19. Chan RW, Titze IR, Titze MR. Further studies of phonation threshold pressure in a physical model of the vocal fold mucosa. J Acoust Soc Am. 1997; 101:3722–3727. [PubMed: 9193059]
20. Zhang Z. Influence of flow separation location on phonation onset. J Acoust Soc Am. 2008; 124:1689–1694. [PubMed: 19045659]
21. Lucero JC. Optimal glottal configuration for ease of phonation. J Voice. 1998; 12:151–158. [PubMed: 9649070]
22. Zhang Z. Cause-effect relationship between vocal fold physiology and voice production in a three-dimensional phonation model. J Acoust Soc Am. 2016; 139:1493. [PubMed: 27106298]
23. Mendelsohn AH, Zhang Z. Phonation threshold pressure and onset frequency in a two-layer physical model of the vocal folds. J Acoust Soc Am. 2011; 130:2961–2968. [PubMed: 22087924]
24. Zhang Z. Dependence of phonation threshold pressure and frequency on vocal fold geometry and biomechanics. J Acoust Soc Am. 2010; 127:2554–2562. [PubMed: 20370037]
25. Zhang Z. On the difference between negative damping and eigenmode synchronization as two phonation onset mechanisms. J Acoust Soc Am. 2011; 129:2163–2167. [PubMed: 21476671]
26. Nasri S, Dulguerov P, Damrose EJ, et al. Relation of recurrent laryngeal nerve compound action potential to laryngeal biomechanics. Laryngoscope. 1995; 105:639–643. [PubMed: 7769950]

27. Shiba TL, Chhetri DK. Dynamics of phonatory posturing at phonation onset. Laryngoscope. 2016; 126:1837–1843. [PubMed: 26690882]

28. Mendelsohn AH, Zhang Z, Luegmair G, et al. Preliminary study of the open quotient in an ex vivo perfused human larynx. JAMA Otolaryngol Head Neck Surg. 2015; 141:751–756. [PubMed: 26181642]

29. Henrich N, D'Alessandro C, Doval B, et al. Glottal open quotient in singing: measurements and correlation with laryngeal mechanisms, vocal intensity, and fundamental frequency. J Acoust Soc Am. 2005; 117(3 pt 1):1417–1430. [PubMed: 15807029]

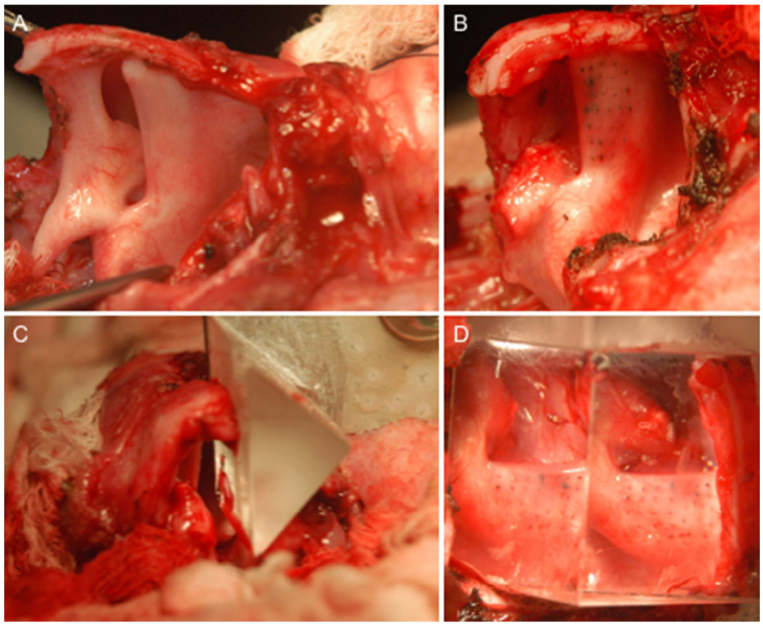

FIGURE 1.

Canine hemilarynx model. **A**. A right vertical hemilaryngectomy has been performed. Sagittal view with trachea (caudal) to the right. **B.** Supraglottic structures have been removed above the level of the laryngeal ventricle. India ink has been used to mark fleshpoints along the medial surface of the left true vocal fold. **C.** Superior view of left hemilarynx apposed to the hypotenuse of a right-angled glass prism. **D.** Sagittal view of the medial surface through the glass prism, showing the two views of the same vocal fold medial surface.

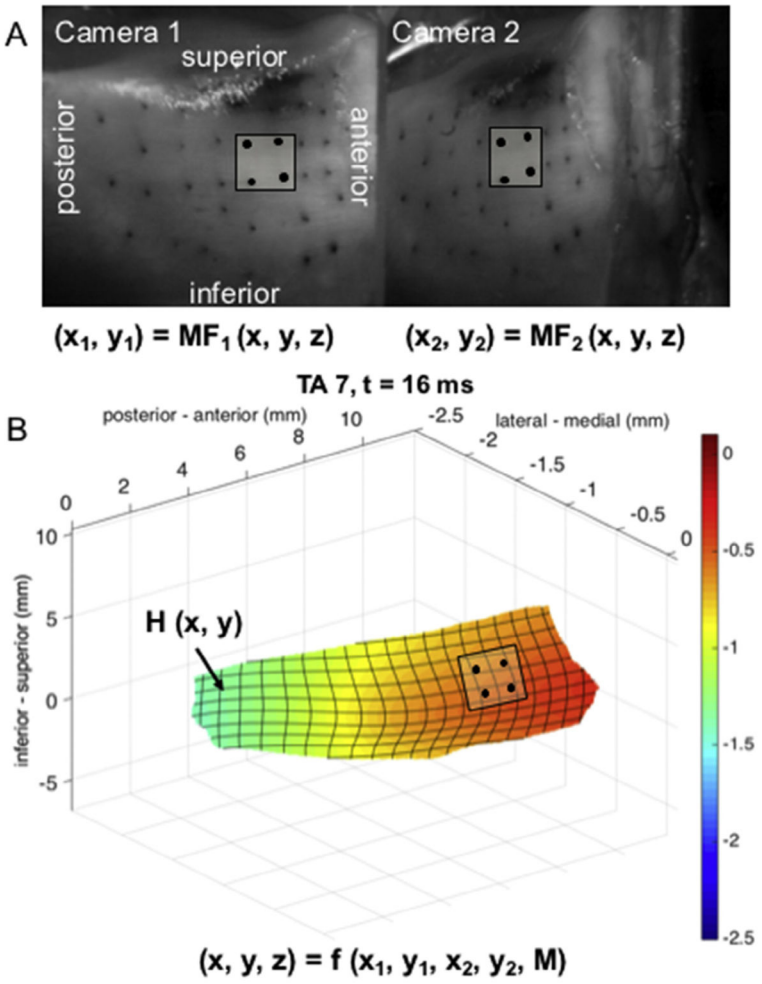

FIGURE 2.

Methodology for 3D deformation calculation. **A.** Raw image of the same vocal fold medial surface showing two camera views seen via right-angled prism. Orientation of the vocal fold is as labeled for the two camera views. The coordinates of a particular area of interest (x, y, z) are mapped to the two cameras (x_1, y_1) and (x_2, y_2). The mapping function (MF) then defines the relationship between the camera coordinates (x_1, y_1, x_2, y_2) and world coordinates (x, y, z). **B.** 3D reconstruction of the vocal fold medial surface plotted from the camera coordinates and the mapping function to determine the surface height, H(x, y).

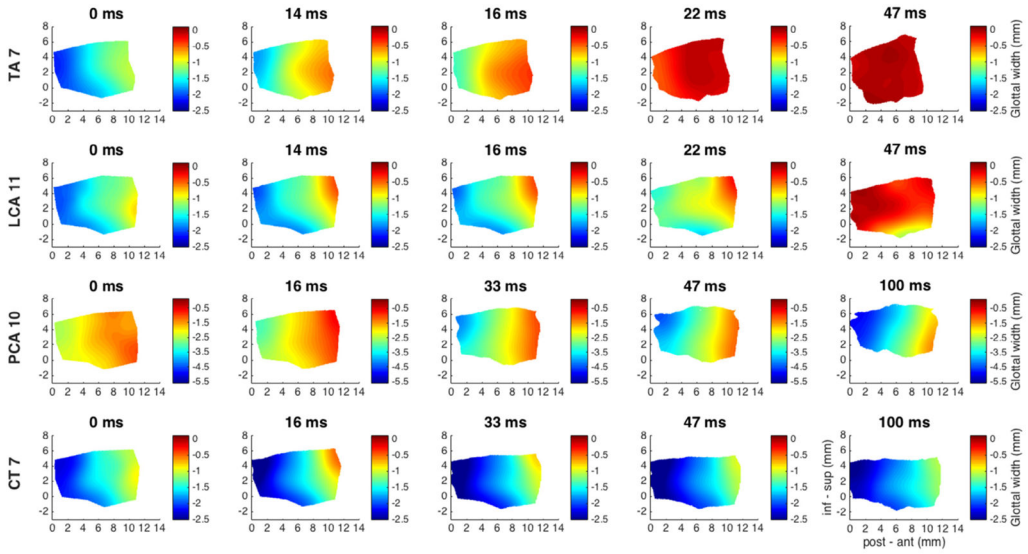

FIGURE 3.

Color-coded 3D contour maps of the vocal fold glottal width (ie, distance of vocal fold medial surface from glottal midline) showing shape changes with activation of each intrinsic laryngeal muscle (ILM). Data are presented in a temporal sequence from resting (left-most column, 0 ms) to final activated posture (rightmost column, 47 or 100 ms). Superior-inferior shape change is shown in the “y” dimension and anterior-posterior shape change is shown in the “x” dimension. Color bar shows degree of the medial surface medial-lateral shape change (glottal width in “z” dimension). ILM activation levels are TA (thyroarytenoid activation grade 7; “TA 7”), LCA (lateral cricoarytenoid activation grade 11; “LCA 11”), PCA (posterior cricoarytenoid activation grade 10; “PCA 10”), and CT (cricothyroid activation grade 7; “CT 7”). inf-sup, inferior to superior; post-ant, posterior to anterior.

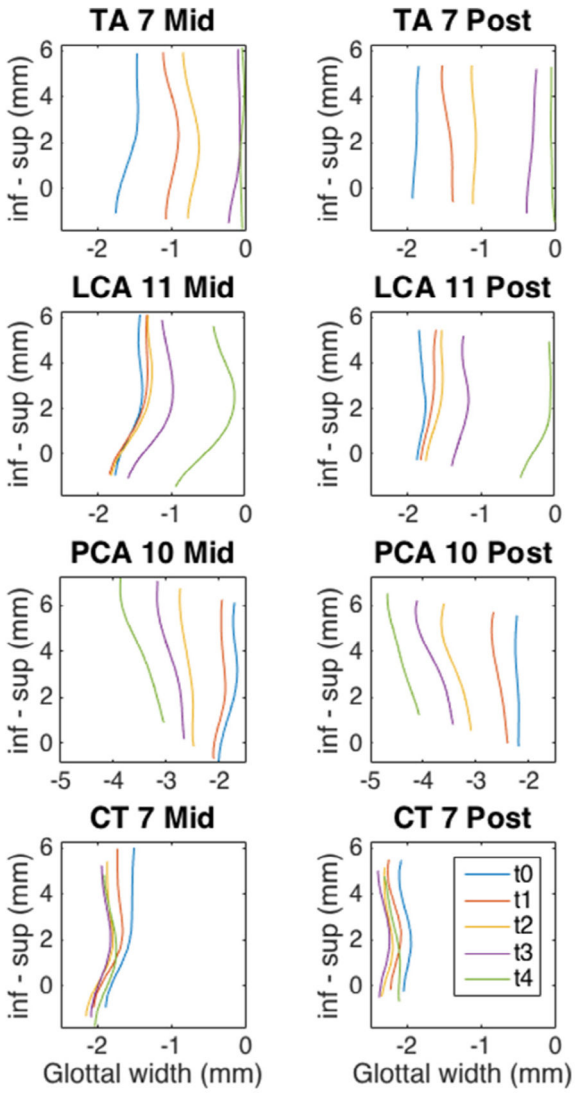

FIGURE 4.

Coronal sections of the vocal fold medial surface for each ILM activation across time. ILM activation levels include: TA (activation grade 7; “TA 7”), LCA (activation grade 11; “LCA 11”), PCA (activation grade 10; “PCA 10”), and CT (activation grade 7; “CT 7”). “Mid” is sectioned through the mid-membranous vocal fold and “post” is sectioned halfway between “Mid” membranous vocal fold and the vocal process. TA activation results in midfold inferior bulge that is faster and more complete than in the posterior glottis. Final posture is rectangular. LCA activation leads to adduction of the vocal fold superior surface with greater adduction at the posterior section. Final posture remains convergent. PCA activation causes abduction and superior displacement of the vocal fold ending with a divergent posture. CT activation shows minimal medial-lateral motion. Temporal sequence matches that of Figure 2; t0–t4 = 0, 14, 16, 22, and 47 ms for TA and LCA, and 0, 16, 33, 47, and 100 ms for PCA and CT. CT, cricothyroid; ILM, intrinsic laryngeal muscle; inf, inferior; LCA, lateral cricoarytenoid; PCA, posterior cricoarytenoid; sup, superior; TA, thyroarytenoid.

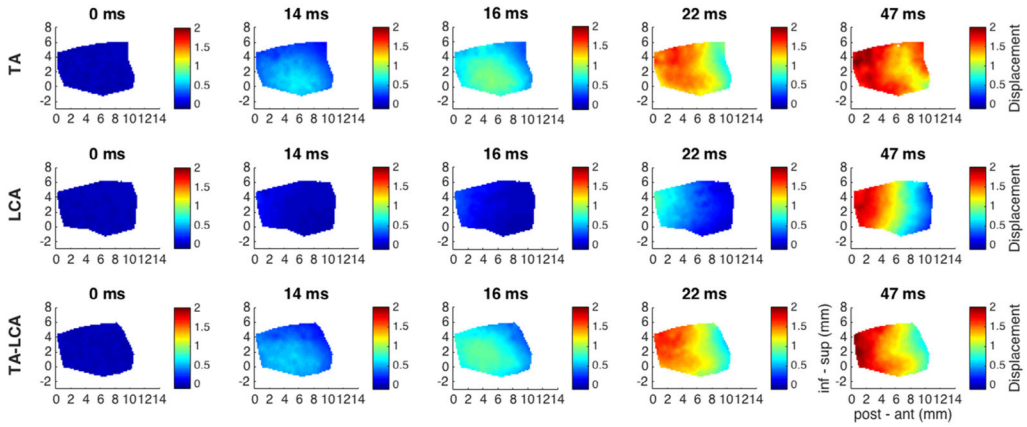

FIGURE 5.

Displacement contour plots for TA, LCA, and combined TA + LCA muscles showing total change in medial surface distance from the glottal midline, relative to baseline posture, in a temporal sequence from baseline to full activation. Inferomedial bulge is noted as prominent feature of maximal TA activation while the posterosuperior edge sees most activity with maximal LCA activation. Combined maximal TA + LCA activation achieves a hybrid result with overall greater adduction seen at the earlier time points (eg, 16 ms) of both the mid and posterior vocal fold. LCA, lateral cricoarytenoid; TA, thyroarytenoid.

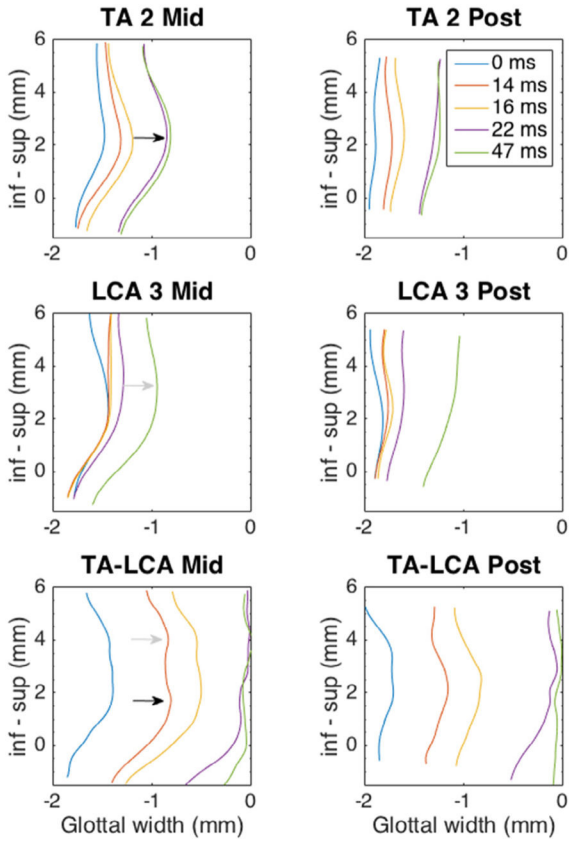

FIGURE 6.

Coronal sections of the medial surface for TA, LCA, and combined TA + LCA activation. Coronal sections of the mid (left column) and posterior (right column) medial surface of the vocal fold for submaximal TA (activation grade 2; “TA 2”), LCA (activation grade 3; “LCA 3”), and combined maximal TA-LCA activation (“TA-LCA”). The TA adducts the mid to inferior aspect of the vocal fold (black arrow) whereas the LCA adducts a more superior portion (gray arrow). Combined maximal TA and LCA activation (black and gray arrows) achieves a more rectangular glottal geometry with increased glottal thickness. inf, inferior; LCA, lateral cricoarytenoid; sup, superior; TA, thyroarytenoid.

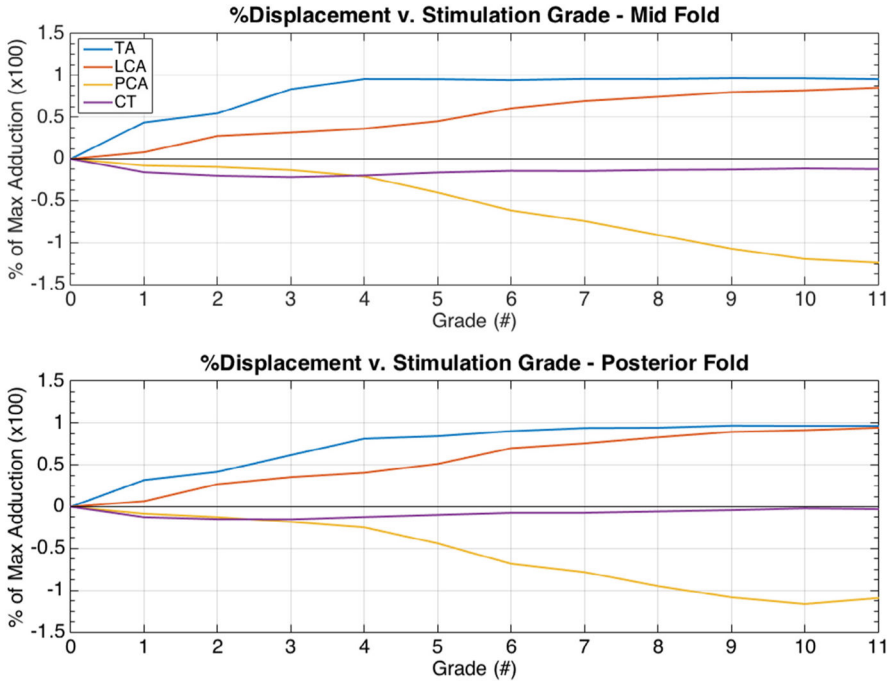

FIGURE 7.

Percent of maximal adduction at the mid **(top)** and posterior **(bottom)** vocal fold for each ILM as a function of graded stimulation. Percent maximal adduction for a given stimulation grade was calculated by dividing final displacement at each level of stimulation by the baseline glottal width (distance to the glottal midline at rest). The TA demonstrates a negative exponential response curve, an early rapid response to increases in graded stimulation, and then reaching a horizontal asymptote much sooner compared to the other ILMs. The LCA and PCA exhibit a more linear response to increases in stimulus level throughout while there is minimal effect on the CT. CT, cricothyroid; ILM, intrinsic laryngeal muscle; LCA, lateral cricoarytenoid; PCA, posterior cricoarytenoid; TA, thyroarytenoid.

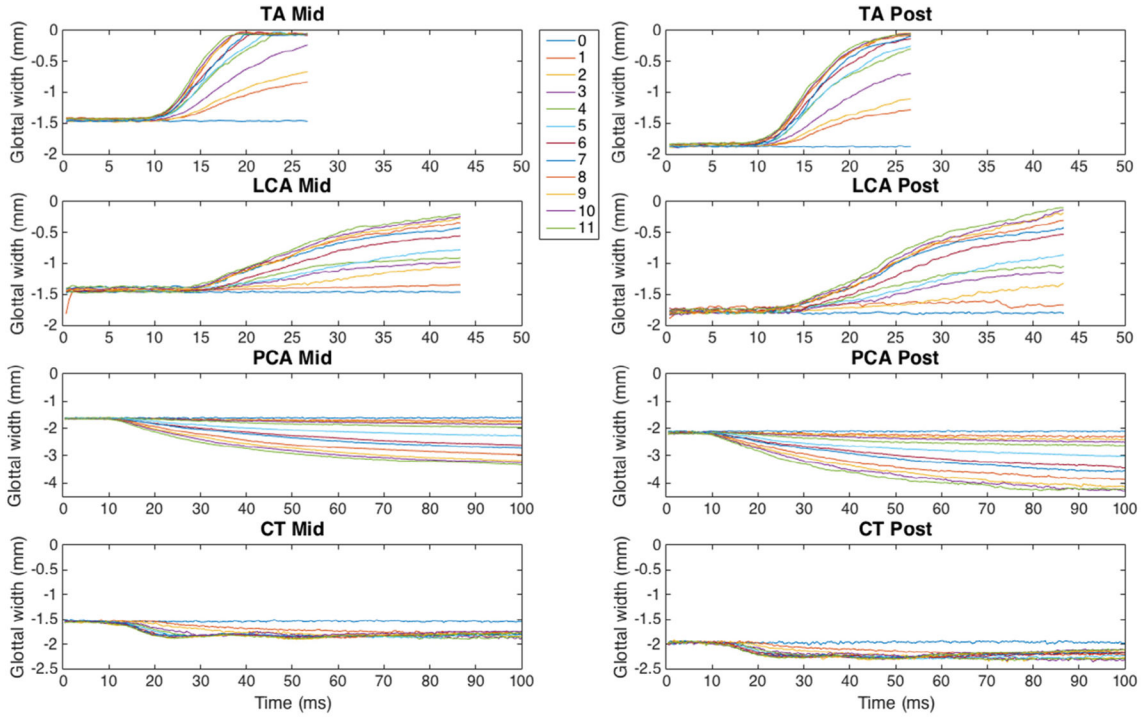

FIGURE 8.

Glottal width as a function of time for each grade of stimulation for each ILM. Each ILM appears to activate with a latency of about 15 ms. The TA is the fastest ILM with a latency around 10 ms and achieving its maximum displacement under 20 ms. The LCA and PCA have a more linear response. There is minimal medial-lateral displacement with CT activation. Overall, a given glottal width can be achieved more rapidly with a larger grade of stimulation (more stimulation current). CT, cricothyroid; ILM, intrinsic laryngeal muscle; LCA, lateral cricoarytenoid; PCA, posterior cricoarytenoid; TA, thyroarytenoid.